ADVANCED FUNCTIONAL MATERIALS
www.afm-journal.de

Materials Views
www.MaterialsViews.com

Morphological Stabilization by Supramolecular Perfluorophenyl-C_{60} Interactions Leading to Efficient and Thermally Stable Organic Photovoltaics

*Ming-Hung Liao, Che-En Tsai, Yu-Ying Lai, Fong-Yi Cao, Jhong-Sian Wu, Chien-Lung Wang, Chain-Shu Hsu, Ian Liau, and Yen-Ju Cheng**

A new $PC_{61}BM$-based fullerene, [6,6]-phenyl-C_{61} butyric acid pentafluorophenyl ester ($PC_{61}BP^F$) is designed and synthesized. This new n-type material can replace $PC_{61}BM$ to form a P3HT:$PC_{61}BP^F$ binary blend or serve as an additive to form a P3HT:$PC_{61}BM$:$PC_{61}BP^F$ ternary blend. Supramolecular attraction between the pentafluorophenyl group of $PC_{61}BP^F$ and the C_{60} cores of $PC_{61}BP^F$/$PC_{61}BM$ can effectively suppress the $PC_{61}BP^F$/$PC_{61}BM$ materials from severe aggregation. By doping only 8.3 wt% $PC_{61}BP^F$, device $PC_{61}BP^F$651 exhibits a PCE of 3.88% and decreases slightly to 3.68% after heating for 25 h, preserving 95% of its original value. When $PC_{61}BP$ with non-fluorinated phenyl group is used to substitute $PC_{61}BP^F$, the stabilizing ability disappears completely. The efficiencies of $PC_{61}BP$651 and $PC_{61}BP$321 devices significantly decay to 0.44% and 0.11%, respectively, after 25 h isothermal heating. Most significantly, this strategy is demonstrated to be effective for a blend system incorporating a low band-gap polymer. By adding only 10 wt% $PC_{61}BP^F$, the PDTBCDTB:$PC_{71}BM$-based device exhibits thermally stable morphology and device characteristics. These findings demonstrate that smart utilization of supramolecular interactions is an effective and practical strategy to control morphological evolution.

1. Introduction

Polymeric solar cells (PSCs) are a promising alternative for clean and renewable energy due to their potential to be fabricated onto large area, light-weight, and flexible substrates by solution processing at a lower cost.[1] Although the concept of bulk heterojunction (BHJ) offers the most straightforward strategy to maximize internal donor–acceptor (D–A) interfacial area for efficient charge separation, tailoring the morphology of the blend in a BHJ device to achieve optimized performance is of pivotal importance and remains rather challenging.[2] Active layers containing poly(3-hexylthiophene) (P3HT) as the electron donor and [6,6]-phenyl-C_{61} butyric acid methyl ester ($PC_{61}BM$) as the electron acceptor are the most widely investigated system with power conversion efficiencies approaching 5% (**Scheme 1**).[1g,2a,3] Thermal annealing of P3HT:$PC_{61}BM$ composite is an effective way to induce maximum interfacial area with higher degree of P3HT crystallinity for efficient charge generation and charge transport.[3b,4] Unfortunately, when thermal treatment at elevated temperature was applied persistently,[5] the kinetically trapped state of the morphology shifted toward the more thermodynamically stable state. The P3HT continued to undergo higher extent of crystallization, while the spherical $PC_{61}BM$ molecules with high molecular mobility gradually diffused out of the polymer matrix and aggregated into larger clusters or single crystals.[5d,5e,6] Such progressive phase-segregation eventually leads to micrometer-sized P3HT:$PC_{61}BM$ domains with dramatic reduction of the interfacial area. Because a photovoltaic device is expected be exposed under long-term sunlight irradiation, the accumulated heat may raise the operational temperature that consequently destroys the optimal morphology and deteriorate the device performance.[7] Several elegant strategies have been developed to stabilize the active layer morphology, such as reduction of crystallinity of polythiophene[8] or fullerene derivatives,[9] increase of T_g of the PPV derivatives,[10] introduction of compatibilizer to impart secondary interactions between the donor and acceptor constitutes,[11] and in situ chemical cross-linking between components in active layers.[12]

Researchers have shown that $PC_{61}BM$ molecules can diffuse rapidly within crystalline P3HT upon thermal treatment, this phenomenon is even more pronounced in an amorphous polymer matrix such as MDMO-PPV.[5c,5d] Restricting the molecular movement of $PC_{61}BM$ to prevent them from severe diffusion would be a straightforward solution to maintain the optimal morphology. Very recently, we developed a $PC_{61}BM$-based derivative, [6,6]-phenyl-C_{61} butyric acid styryl ester (PCBS), containing a polymerizable styrene group.[12f] The $PC_{61}BM$:P3HT blend system was added with a small amount of PCBS that can undergo in situ thermal polymerization to suppress the thermal-driven aggregation of the fullerene

M.-H. Liao, C.-E. Tsai, Dr. Y.-Y. Lai, F.-Y. Cao, Dr. J.-S. Wu. Prof. C.-L. Wang, Prof. C.-S. Hsu, Prof. I. Liau, Prof. Y.-J. Cheng
Department of Applied Chemistry
National Chiao Tung University
1001 Ta Hsueh Road Hsin-Chu, 30010, Taiwan
E-mail: yjcheng@mail.nctu.edu.tw

DOI: 10.1002/adfm.201300437

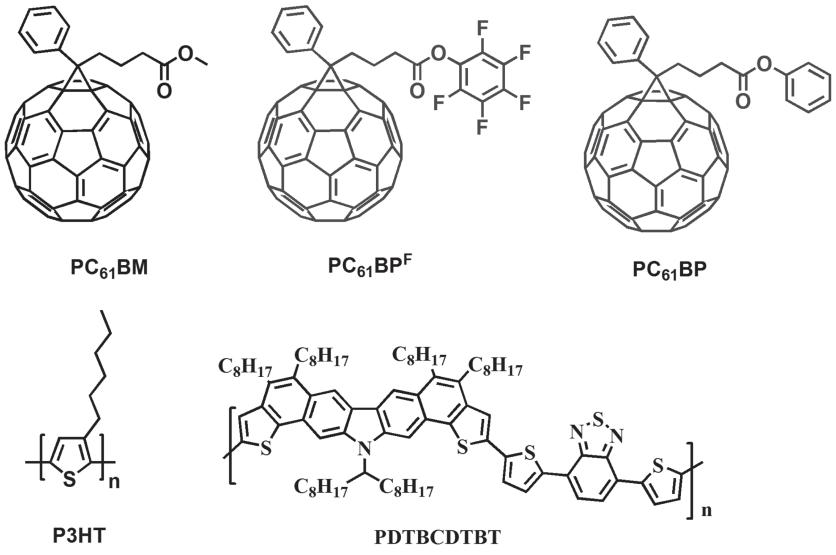

Scheme 1. Chemical structures of $PC_{61}BM$, $PC_{61}BP^F$, $PC_{61}BP$, P3HT, and **PDTBCDTBT** copolymer used in this research.

materials, thereby the optimized morphology can be preserved through the covalent fixation. Although the concept of covalent locking is proved to be effective, the success of this strategy is critically dependent on manipulating the temperature window to control the occurrence of polymerization. Initiation of thermal-induced polymerization must not occur before the optimized morphology is developed. Undesired polymerization at the early stage will sterically interrupt the molecular assembly of P3HT and $PC_{61}BM$ during the morphological evolution.

Beyond thermal-induced polymerization in bulk, morphological engineering involving noncovalent self-assembly emerges as a new exploratory direction for modulating morphology. Introducing small amount of additives into active layers to assist physically the formation of suitable nano-morphology has been extensively investigated.[13] Despite of substantial success of this strategy in improving efficiency, understanding the mechanism of morphological evolution is still lacking. Hydrogen bonding approach is widely used for self-assembly.[14] However, the complementary groups with high polarity for H-bonding formation are known to have negative effect on charge transport. Therefore, so far this strategy has not been successful.[15] It was documented that a 1:1 mixture of benzene/hexafluorobenzene adopts a face-to-face stacking with an alternating sequence.[16] This stacking arrangement is due to complementary attractions between benzene and hexafluorobenzene. The stabilization energy of this attraction is estimated to be 4.3 kcal mol^{-1} and the cofacial distance between two planar structures is about 3.7 Å.[16e] Such physical interactions have been observed in various aromatic/perfluoroaromatic systems that create a variety of fascinating molecular assemblies.[16b–16h] In a very similar manner, perfluorophenyl motif has a favorable interaction with the surface of a fullerene that actually contains 20 hexagonal rings with more localized electrons. It has been demonstrated that through such a face-to-face C_6F_5–fullerene interaction, 1,4-bis(pentafluorobenzenyl) fullerene assembles into an interlocked one-dimensional zigzag array in the solid state.[17] Inspired by this work, we envision that the C_6F_5–C_{60} physical interaction could be smartly utilized to substitute the function of chemical polymerization for achieving morphological stabilization. To demonstrate this strategy, we designed and synthesized a new $PC_{61}BM$-based fullerene, [6,6]-phenyl-C_{61} butyric acid pentafluorophenyl ester ($PC_{61}BP^F$, Scheme 1). The structural difference between $PC_{61}BM$ and $PC_{61}BP^F$ is that the methyl group in $PC_{61}BM$ is replaced by a pentafluorophenyl group in $PC_{61}BP^F$. This small modification not only makes $PC_{61}BP^F$ maintain intrinsic properties of $PC_{61}BM$ but also imparts C_6F_5–C_{60} interaction between $PC_{61}BP^F$ molecules. For comparison, we also synthesized a reference compound, [6,6]-phenyl-C_{61} butyric acid phenyl ester ($PC_{61}BP$), which has an identical chemical structure to $PC_{61}BP^F$ except that the pentafluorophenyl in $PC_{61}BP^F$ is changed to a non-fluorinated phenyl analogue (Scheme 1).

The $PC_{61}BP^F$ can be used as an acceptor to form a P3HT:$PC_{61}BP^F$ binary blend, or be added into a P3HT:$PC_{61}BM$ system to form a P3HT:$PC_{61}BM$:$PC_{61}BP^F$ ternary blend. Regardless of using binary or ternary blends, the devices incorporating $PC_{61}BP^F$ exhibited stable or enhanced device characteristics during long-term thermal treatment. In sharp contrast, the devices employing non-fluorinated $PC_{61}BP$ do not show the ability of morphological stabilization upon thermal heating. We have successfully demonstrated that the smartly utilization of supramolecular physical interaction is a simple and feasible approach to control nano-morphology leading to efficient and stable organic photovoltaics.

2. Results and Discussion

2.1. Synthesis and Thermal Properties of the Pentafluorophenol and Phenol-Functionalized $PC_{61}BM$ Derivatives

$PC_{61}BP^F$ and $PC_{61}BP$ were easily prepared by the esterification of [6,6]-phenyl-C_{61} butyric acid ($PC_{61}BA$) with pentafluorophenol and phenol, respectively, in the presence of 1-ethyl-3-(3-dimethylaminopropyl) carbodiimide (EDC) and 4-dimethylaminopyridine (DMAP) in 42% yield (**Scheme 2**). Thermogravimetric analysis (TGA) measurement and differential scanning calorimetry (DSC) were used to measure the thermal properties of $PC_{61}BP^F$ molecule (Figures S1,S2, Supporting Information). Both of $PC_{61}BP^F$ and $PC_{61}BM$ exhibited a melting point which is indicative of their crystalline nature. $PC_{61}BP^F$ exhibits almost identical absorption spectrum and similar cyclic voltammetry curve to $PC_{61}BM$ (Figures S3,S4, Supporting Information), indicating that pentafluorophenol group does not have influence on these intrinsic properties.

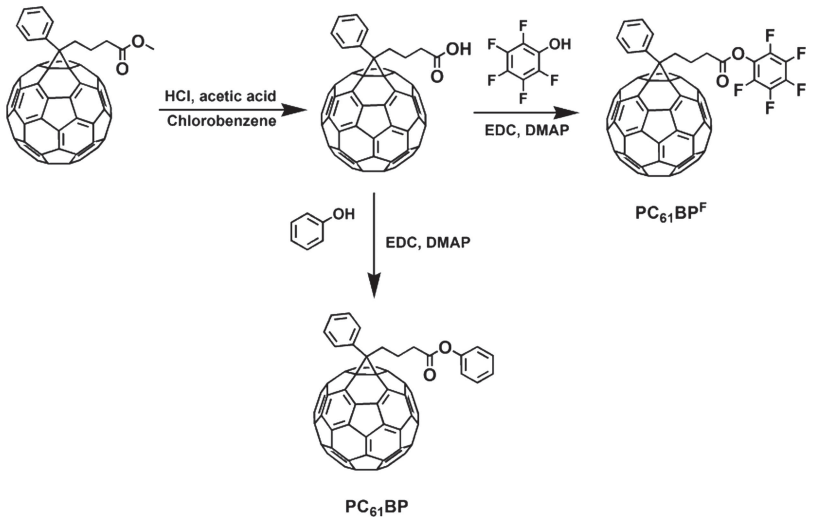

Scheme 2. The synthetic route for $PC_{61}BP$ and $PC_{61}BP^F$.

2.2. Performance and Morphological Stability

In this research, we employed a conventional device configuration (ITO/PEDOT:PSS/active layer/Ca/Al) where all the spin-coated active layer blends were thermally annealed at 140 °C for 15 min. This is a standard condition used to develop suitable morphology for traditional P3HT:$PC_{61}BM$ system. To evaluate the multiple functions of $PC_{61}BP^F$ to serve as an acceptor material, $PC_{61}BP^F$ was incorporated into P3HT:$PC_{61}BM$ blend to form a ternary system. For simplicity, $PC_{61}BP^F$xyz abbreviation is used to denote a ternary blend system where *x*, *y*, and *z* represent the relative weight ratio of P3HT:$PC_{61}BM$:$PC_{61}BP^F$, respectively. For comparison, we first fabricated a $PC_{61}BP^F110$ reference device with a P3HT:$PC_{61}BM$:$PC_{61}BP^F$ (1:1:0 in wt%) blend that delivered a PCE of 4.08% under AM 1.5G illumination at 100 mW cm^{-2}. We then fabricated a $PC_{61}BP^F101$ device using a P3HT:$PC_{61}BM$:$PC_{61}BP^F$ blend (1:0:1 in wt%) as the active layer where $PC_{61}BM$ is completely replaced by $PC_{61}BP^F$. Under AM 1.5G illumination at 100 mW cm^{-2}, $PC_{61}BP^F101$ device showed a relatively lower PCE of 2.50%. This primary result implies that the electron mobility of $PC_{61}BP^F$ might be lower than that of $PC_{61}BM$, or the morphology of P3HT:$PC_{61}BP^F$ blend is not optimized for charge transport. To potentially improve the electron-transporting properties in the composite, we incorporated $PC_{61}BM$ into the P3HT:$PC_{61}BP^F$ blend to dilute the $PC_{61}BP^F$ content and thus form a ternary blend system. Considering that the structures of $PC_{61}BM$ and $PC_{61}BP^F$ are very similar, $PC_{61}BP^F$ should be physically compatible with $PC_{61}BM$ in mixed solid state. We fixed the blending weight ratio of P3HT to the total n-type materials (i.e., $PC_{61}BM$ plus $PC_{61}BP^F$) as 1:1 but the relative content between $PC_{61}BM$ and $PC_{61}BP^F$ can be adjustable. Device $PC_{61}BP^F211$ (P3HT:$PC_{61}BM$:$PC_{61}BP^F$ = 2:1:1 in wt%), device $PC_{61}BP^F321$ (P3HT:$PC_{61}BM$:$PC_{61}BP^F$ = 3:2:1 in wt%) and device $PC_{61}BP^F651$ (P3HT:$PC_{61}BM$:$PC_{61}BP^F$ = 6:5:1 in wt%) were therefore fabricated. Under the identical conditions, the efficiencies were indeed improved to 3.18% for device $PC_{61}BP^F321$ and 3.20% for device $PC_{61}BP^F211$, respectively. Furthermore, the device $PC_{61}BP^F651$ with the lowest $PC_{61}BP^F$ content showed a much improved PCE of 3.88%. To systematically evaluate the $PC_{61}BP^F$'s effect on morphological evolution under influence of thermal treatment, we fabricated a series of analogous devices $PC_{61}BP^F110$, $PC_{61}BP^F651$, $PC_{61}BP^F321$, $PC_{61}BP^F211$, and $PC_{61}BP^F101$ where the corresponding active layers, initially thermally annealed at 140 °C for 15 min, were further subjected to isothermal heating at 150 °C for 5, 10, 15, 20, and 25 h prior to the deposition of top electrodes. The *J*–*V* curves of all the devices are shown in the **Figure 1**, and their corresponding photovoltaic parameters (PCE, V_{oc}, J_{sc}, and FF) as a function of heating time at 150 °C are summarized in **Table 1** and plotted in **Figure 2** (see Tables S1–S4, Supporting Information, for more detailed data). It was found that the performance of $PC_{61}BP^F110$ reference device decreases as the heating time increases. The PCE of the device dropped dramatically from 4.08% to 0.69% after 25 h isothermal heating. The decreased efficiency is mainly a result of the decrease of J_{sc} value. Encouragingly, the efficiency of the $PC_{61}BP^F101$ devices does not decrease at all as the heating time increases. In contrast, the PCE values were gradually improved from 2.5% to 3.34% after 25 h heating. In a similar manner, the $PC_{61}BP^F211$ devices exhibited steady improvement of PCE values from 3.2% to 3.43%, while the $PC_{61}BP^F321$ devices also showed improved performance from 3.18% to 3.7% after 25 h isothermal heating. Interestingly, the device $PC_{61}BP^F651$ showed slight decrease of PCE values from 3.88% to 3.68%. These results indicated that the morphological evolution of the active layers is highly dependent on the relative blending ratio of $PC_{61}BM$ and $PC_{61}BP^F$. In the P3HT:$PC_{61}BM$ system ($PC_{61}BP^F110$), the optimized morphology for high performance can be rapidly achieved by moderate thermal annealing (i.e., 140 °C for 15 min). However, when heating is applied constantly, this optimized morphology is also easily deteriorated due to the continuous phase separation toward the thermodynamically stable state.

In contrast, the presence of $PC_{61}BP^F$ greatly suppresses the tendency of the fullerene fraction (i.e., $PC_{61}BM$ and $PC_{61}BP^F$) toward aggregation. To demonstrate the existence of C_6F_5–C_{60} interaction, we used $PC_{61}BP$ with non-fluorinated phenyl group to substitute $PC_{61}BP^F$ and fabricated $PC_{61}BP651$ and $PC_{61}BP321$ devices under otherwise identical conditions. The *J*–*V* curves of all the devices are shown in **Figure 3**, and their corresponding photovoltaic parameters as a function of heating time at 150 °C were plotted in **Figure 4** and summarized in Table 1 (see Tables S5,S6, Supporting Information, for more detailed data). Initially, device $PC_{61}BP651$ yielded a PCE of 3.45%. Unlike the case of $PC_{61}BP^F651$, the performance of $PC_{61}BP651$ degraded significantly to 0.63% only after 5 h heating at 150 °C, and continued to decrease to 0.44% after 25 h heating. Similarly, device $PC_{61}BP321$ delivered a PCE of 2.23% in the first place but dropped to a PCE of 0.11% with a very poor J_{sc} of 0.73 mA cm^{-2} after 25 h thermal treatment. The decay of J_{sc} and V_{oc} values is

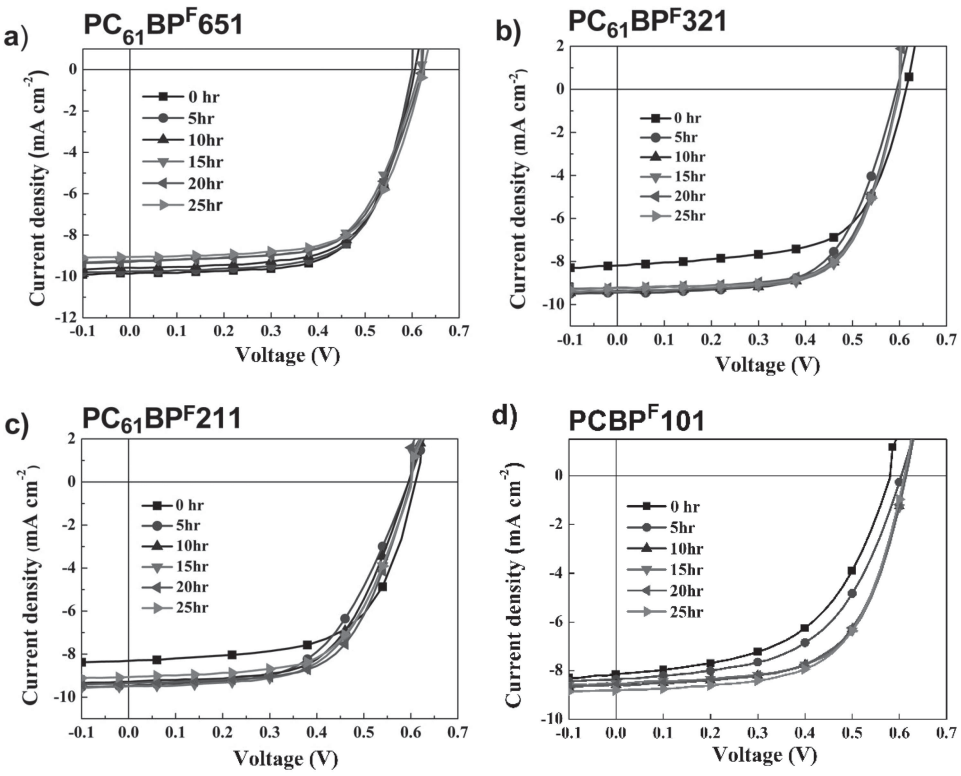

Figure 1. *J–V* characteristics of PSCs based on a) $PC_{61}BP^F651$, b) $PC_{61}BP^F321$, c) $PC_{61}BP^F211$, and d) $PC_{61}BP^F101$ blends before and after isothermal heating at 150 °C for various periods of time.

the major reason accounting for the low PCEs. These behaviors clearly demonstrate that the presence of pentafluorophenyl group in $PC_{61}BP^F$ to exert C_6F_5–C_{60} interactions plays a decisive role in controlling and stabilizing the morphology against thermal heating.

Table 1. Photovoltaic parameters of PSCs (ITO/PEDOT:PSS/active layer/Ca/Al) before and after isothermal heating at 150 °C for 25 h.

Devices	Time [h]	V_{oc} [V]	J_{sc} [mA cm^{-2}]	FF [%]	PCE [%]
$PC_{61}BP^F110$	0	0.60	–10.26	66	4.08
$PC_{61}BP^F110$	25	0.62	–2.27	49	0.69
$PC_{61}BP^F651$	0	0.60	–9.87	65.60	3.88
$PC_{61}BP^F651$	25	0.62	–9.06	65.47	3.68
$PC_{61}BP^F321$	0	0.62	–8.19	62.35	3.18
$PC_{61}BP^F321$	25	0.60	–9.24	66.66	3.70
$PC_{61}BP^F211$	0	0.62	–8.20	60.72	3.20
$PC_{61}BP^F211$	25	0.60	–9.05	63.15	3.43
$PC_{61}BP^F101$	0	0.58	–8.15	52.94	2.50
$PC_{61}BP^F101$	25	0.62	–8.81	61.05	3.34
$PC_{61}BP651$	0	0.60	–8.92	64.40	3.45
$PC_{61}BP651$	25	0.60	–1.78	41.68	0.44
$PC_{61}BP321$	0	0.58	–6.62	58.05	2.23
$PC_{61}BP321$	25	0.50	–0.73	30.06	0.11

2.3. Optical Microscopy and Atomic Force Microscopy

Optical microscopy (OM) was used to investigate the morphological alteration of the blends in size of micrometer under the influence of heating (**Figure 5**). Thermal annealing of the P3HT:$PC_{61}BM$ blend at 150 °C for 25 h induced a severe macrographic alteration, forming the needle-shaped $PC_{61}BM$ crystals of hundreds micrometers in length.[5e,5f,12f] In contrast, the morphologies of the $PC_{61}BP^F321$, $PC_{61}BP^F211$, and $PC_{61}BP^F101$ blend remain almost unchanged before and after thermal annealing, demonstrating the physical C_6H_5–C_{60} interactions of $PC_{61}BP^F$ show excellent ability to prevent the morphologies from undergoing phase separation. However, $PC_{61}BP^F651$ blend with the lowest $PC_{61}BP^F$ content shows less ability to lock the morphology. The OM image of $PC_{61}BP^F651$ exhibited a slight macrographic alteration with observable needle-shaped crystals in some local areas after 25 h heating. This morphological change is also consistent with the slight reduction in PCE of the $PC_{61}BP^F651$ device. It should be emphasized that the OM image of $PC_{61}BP651$ blend showed extensive phase separation after 25 h heating, meaning that $PC_{61}BP$ without pentafluorophenyl group has no effect on morphological stabilization.

Atomic force microscopy (AFM) was also used to observe the evolution of the surface morphology before and after 25 h heating at 150 °C (Figure S5, Supporting Information). The surface roughness of height image of $PC_{61}BP^F651$ blend increased from 1.01 nm to 4.92 nm after 25 h heating, indicating some degree of morphology alternation, which is also consistent with

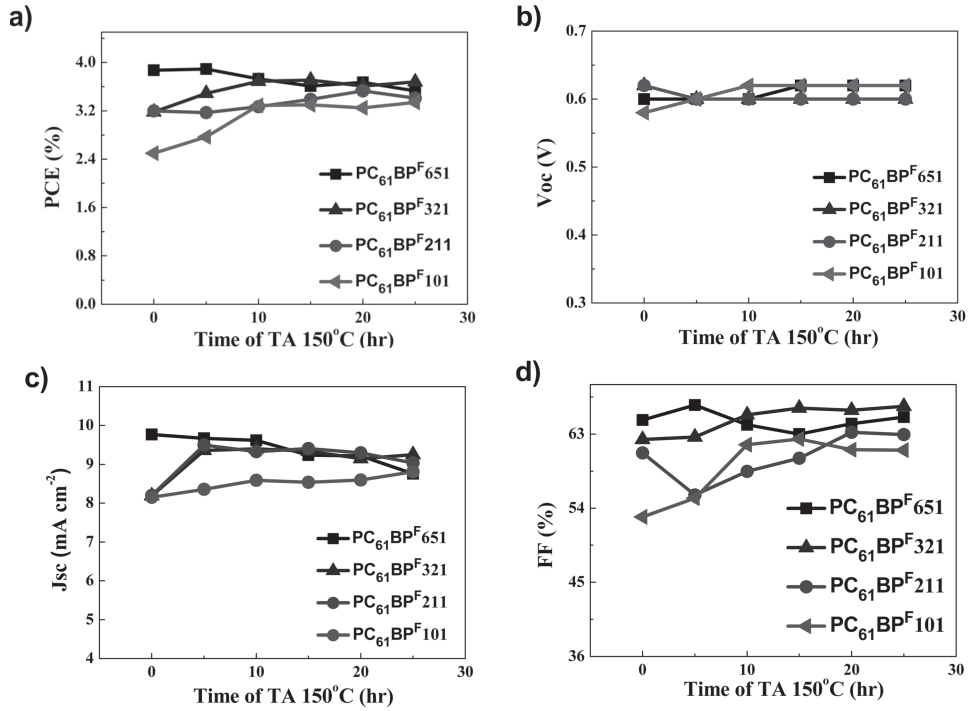

Figure 2. Photovoltaic parameters of PSCs based on the $PC_{61}BP^F651$, $PC_{61}BP^F321$, $PC_{61}BP^F211$, and $PC_{61}BP^F101$ blends as a function of heating time at 150 °C. a) PCE, b) open-circuit voltage (V_{oc}), c) short-circuit current (J_{sc}), and d) fill factor (FF).

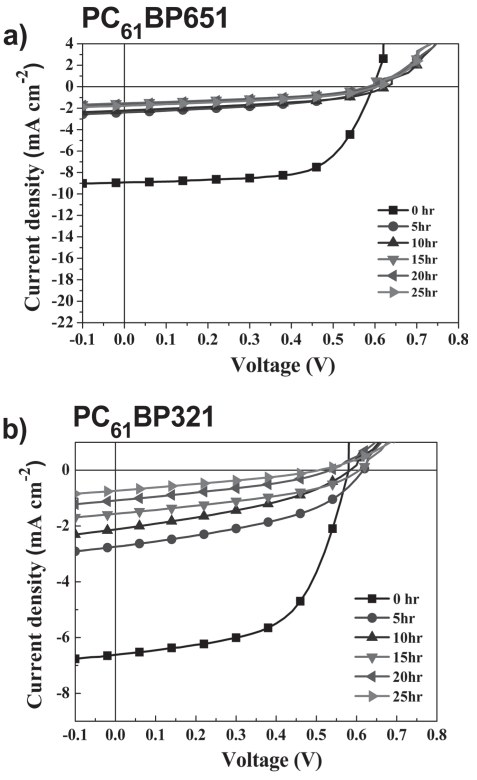

Figure 3. *J–V* characteristics of PSCs based on a) $PC_{61}BP651$, b) $PC_{61}BP321$ blends before and after isothermal heating at 150 °C for various periods of time.

the optical microscopy image of $PC_{61}BP^F651$ thin film. However, other ternary $PC_{61}BP^F321$, $PC_{61}BP^F211$, and $PC_{61}BP^F101$ systems with higher content of $PC_{61}BP^F$ showed marginal increases of roughness after thermal treatment. This observation suggests that these morphologies are generally stable, and the slightly increased roughness might be indicative of the increased P3HT crystallinity. Nevertheless, the $PC_{61}BP651$ blend without C_6F_5–C_{60} interaction showed a significant increase of roughness from 4.60 to 7.71 nm.

2.4. X-Ray Diffraction Measurements

To gain more insight into the morphological evolution, three representative $PC_{61}BP^F110$, $PC_{61}BP^F101$, and $PC_{61}BP^F321$ blending systems were selected for wide angle X-ray diffraction (WAXRD) investigation. After taking the first XRD measurement of the as-cast films, each pristine film was annealed at 150 °C for 25 h followed by the second measurement to monitor the thermal-induced structural changes in the films, as shown in **Figure 6**. Three diffraction peaks located at 2θ = 5.3° (*d*-spacing: 1.67 nm), 10.7° (*d*-spacing: 8.3 Å) and 15.8° (*d*-spacing: 5.6 Å) were observed for all the as-cast films of $PC_{61}BP^F110$, $PC_{61}BP^F101$, and $PC_{61}BP^F321$ blends. These three diffractions with scattering vector (q) ratio of 1:2:3 are an indication of the presence of a long-range ordered lamellar structure. The *d*-spacing of the first diffraction peak fits closely with the *a* dimension of the monoclinic unit cell of the crystalline P3HT.[18] Thus, the three diffraction peaks can be indexed as the (100), (200), and (300) diffractions of P3HT. For comparison,

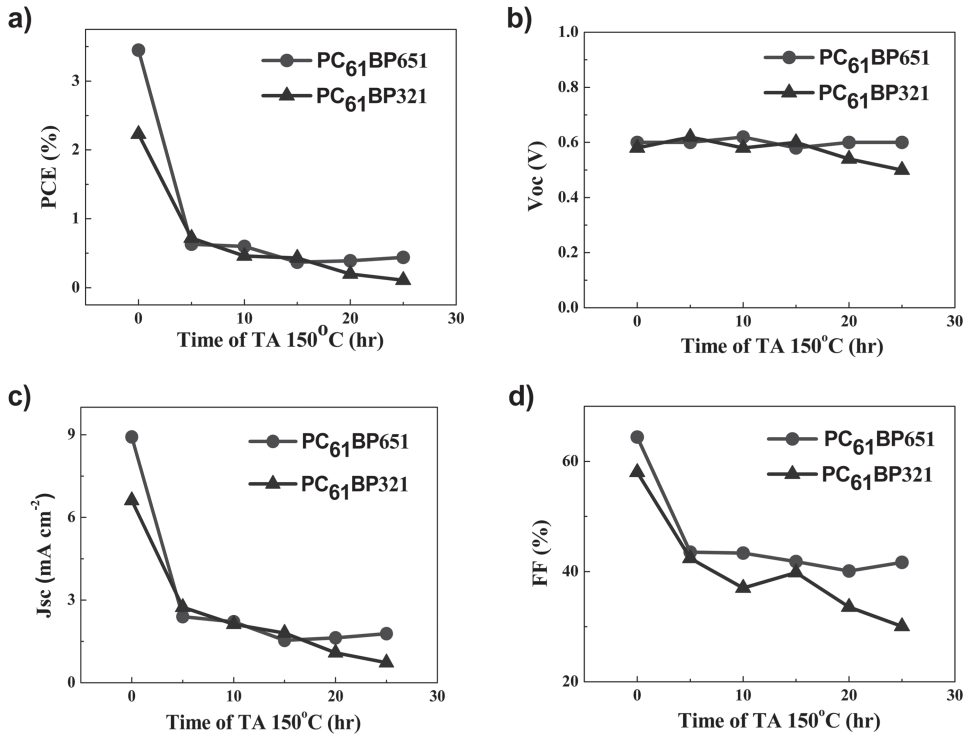

Figure 4. Photovoltaic parameters of PSCs based on the $PC_{61}BP651$ and $PC_{61}BP321$ blends as a function of heating time at 150 °C. a) PCE, b) open-circuit voltage (V_{oc}), c) short-circuit current (J_{sc}), and d) fill factor (FF).

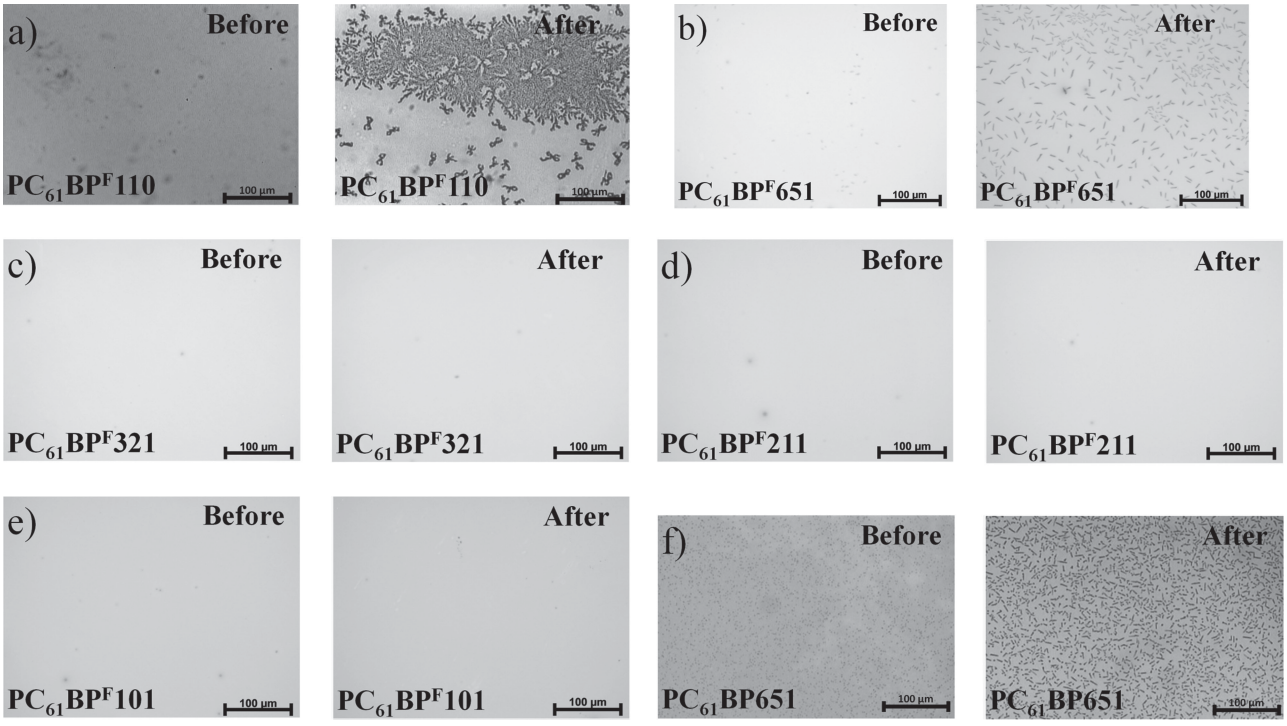

Figure 5. OM images of the blends before and after isothermal heating at 150 °C for 25 h for a) $PC_{61}BP^{F}110$, b) $PC_{61}BP^{F}651$, c) $PC_{61}BP^{F}321$, d)$PC_{61}BP^{F}211$, e) $PC_{61}BP^{F}101$, and f) $PC_{61}BP651$.

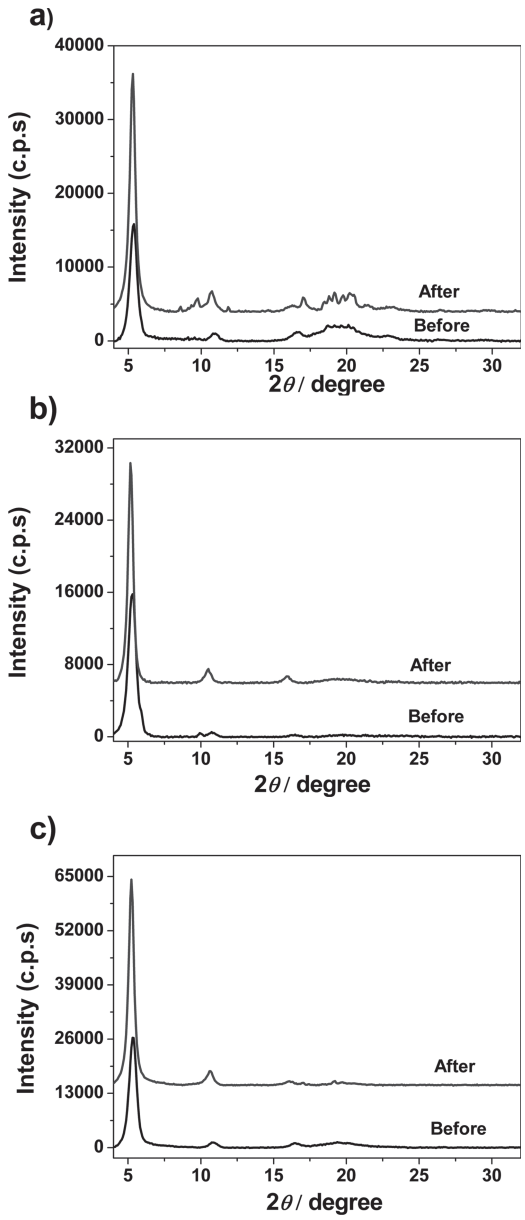

Figure 6. 1D WAXD patterns of a) $PC_{61}BP^F110$, b) $PC_{61}BP^F101$, and c) $PC_{61}BP^F321$ drop-cast films. The patterns of each film were measured before and after thermal annealing at 150 °C for 25 h.

the XRD measurement of pure $PC_{61}BM$ as well as $PC_{61}BP^F$ cast films was also performed, respectively (Figure S6, Supporting Information). The multiple diffraction peaks observed in the patterns indicate that both $PC_{61}BM$ and $PC_{61}BP^F$ are crystalline in their pristine films. These characteristic peaks of crystalline $PC_{61}BM$ and $PC_{61}BP^F$ were unobservable in the as-cast samples, which indicate that the presence of P3HT chains strongly hinders the crystallization of the $PC_{61}BM$ and $PC_{61}BP^F$ during the solvent evaporation process.[19] After thermal annealing of the $PC_{61}BP^F110$ blend at 150 °C for 25 h, the intensities of (100), (200), and (300) diffractions of P3HT were enhanced significantly (Figure 6a).[20] More importantly, the annealing process also led to the emergence of diffraction peaks near $2\theta = 9°$ and from 17 to 23°. By matching with the diffraction pattern of the pristine $PC_{61}BM$, the additional peaks were identified as the formation of crystalline domain of $PC_{61}BM$ (Figure S5, Supporting Information). In contrast, upon thermal treatments, $PC_{61}BP^F101$ and $PC_{61}BP^F321$ blends (Figure 6b,c) only exhibited more pronounced P3HT patterns without showing distinguishable crystalline diffractions of either $PC_{61}BM$ or $PC_{61}BP^F$. Based on the XRD analysis, several points should be noted. First, thermal treatment gradually induces higher degree of P3HT crystallinity regardless of the composition of n-type materials. Second, in the presence of $PC_{61}BP^F$, thermal-induced aggregation of $PC_{61}BP^F$ in the $PC_{61}BP^F101$ binary blend, or $PC_{61}BP^F/PC_{61}BM$ in the $PC_{61}BP^F321$ ternary blend is suppressed, which is in contrast to that from the $PC_{61}BP^F110$ system showing severe P3HT:$PC_{61}BM$ phase separation. The XRD data again confirm the effectiveness of the $PC_{61}BP^F$ in hindering the crystallization of fullerene-based materials in the active layers.

2.5. The Carrier Mobilities in the Blends

To quantify the influence of the $PC_{61}BP^F$ on the charge transporting characteristics in the active layers, we fabricated unipolar devices to independently evaluate the hole (**Figure 7**) and electron mobilities (**Figure 8**) of $PC_{61}BP^F651$, $PC_{61}BP^F321$, $PC_{61}BP^F211$, and $PC_{61}BP^F101$ blends before and after 25 h heating at 150 °C by space-charge-limited current (SCLC) technique (**Table 2**). It was found that all hole mobilities of $PC_{61}BP^F651$, $PC_{61}BP^F321$, $PC_{61}BP^F211$, and $PC_{61}BP^F101$ were increased to some degree after 25 h heating. These results suggest that the thermal annealing drives P3HT to align and form higher crystallinity. However, the electron mobilities of $PC_{61}BP^F321$ and $PC_{61}BP^F211$ blends were increased slightly after 25 h heating. The $PC_{61}BP^F101$ device containing 100% $PC_{61}BP^F$ as the n-type material exhibited improved electron mobility by 1.8 times after 25 h thermal annealing.

2.6. Theoretical Calculations

In order to investigate the extra stabilization brought by the pentafluorophenyl group of $PC_{61}BP^F$, quantum-chemical calculations were carried out. Geometry optimizations were performed with the Gaussian09 suite at the wB97XD/6–311G(d,p) level of theory. Specifically, the wB97XD functional, which contains empirical dispersion-energy correction, has been demonstrated to be effective in describing the weak intermolecular interaction.[21] With consideration of reducing large consumption of computational time, pristine C_{60} and methyl perfluorobenzoate (BP^F) were used as simplified model compounds for studying the interactions between fullerenes and fluorinated aromatic esters. The computational results reveal that C_{60} can interact with BP^F to form a stable complex $C_{60}BP^F$. As illustrated in **Figure 9**, the optimized structure of $C_{60}BP^F$ exhibits that BP^F is situated approximately above the 5–6 and 6–6 edges of C_{60} and the average distance between

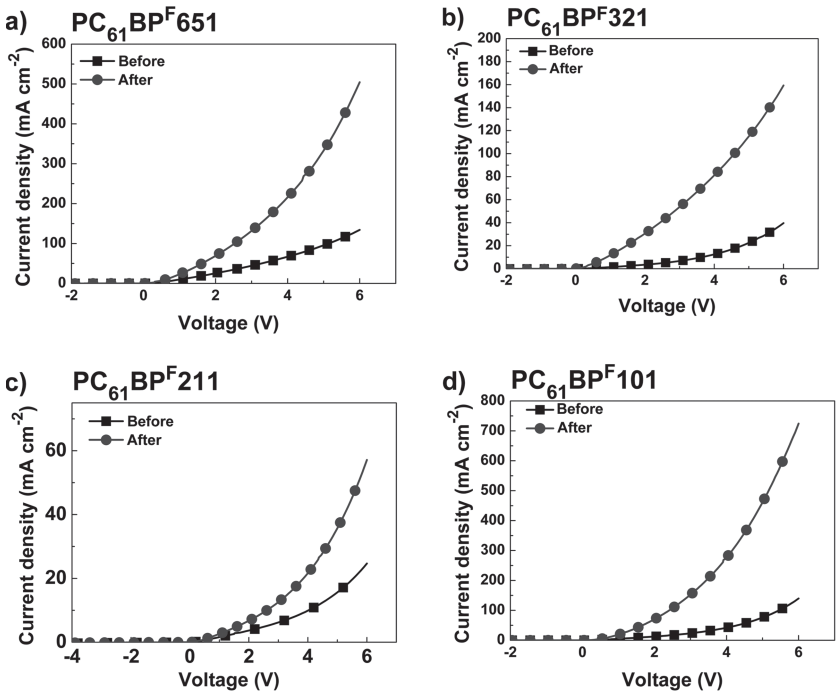

Figure 7. Hole-only devices for a) $PC_{61}BP^F651$, b) $PC_{61}BP^F321$, c) $PC_{61}BP^F211$, and d) $PC_{61}BP^F101$ blends before and after thermal annealing at 150 °C for 25 h.

C_{60} and BP^F is ≈3.21 Å. The strength of this intermolecular interaction can be further quantified by the bonding energy (association energy), –10.58 kcal mol^{-1}, of the resultant complex. Subsequently, computational energy decomposition analysis (ETS-NOCV)[21] of the C_{60}/BP^F interaction was performed to elucidate the stabilization energy brought by the fluorinated phenyl group.[22] For more information about ETS-NOCV analysis, one can consult the publications listed in reference [21]. ETS-NOCV analysis was conducted with the ADF suite using BP86-BJDAMP/TZP. The incorporation of BJ damping into the BP86 functional provides dispersion-energy correction and has been demonstrated to give better results for medium to long-range intermolecular interactions.[23] As listed in **Table 3**, the bonding energy (ΔE) calculated with BP86-BJDAMP/TZP is slightly greater than that obtained with wB97XD/6–311G(d,p). The bonding energy ΔE consists of two contributions: the preparation energy ΔE_{prep} and the interaction energy ΔE_{int}. ΔE_{int} can be further decomposed into four chemically meaningful components, electrostatic interaction (ΔV_{elst}), Pauli repulsion (ΔE_{pauli}), orbital interaction (ΔE_{oi}), and dispersion (ΔE_{dis}). A more detailed description of these interactions is summarized in supporting information. For $C_{60}BP^F$, 59% of the total stabilization energy comes from the dispersion-energy term (ΔE_{dis}) and the electrostatic interaction and the orbital interaction have contributions of 23% and 18%, respectively. It is evident that the additional stabilization energy comes mostly from the dispersion energy, which is the van der Waals interaction between C_{60} and BP^F. However, electrostatic and orbital interactions still have noticeable contributions.

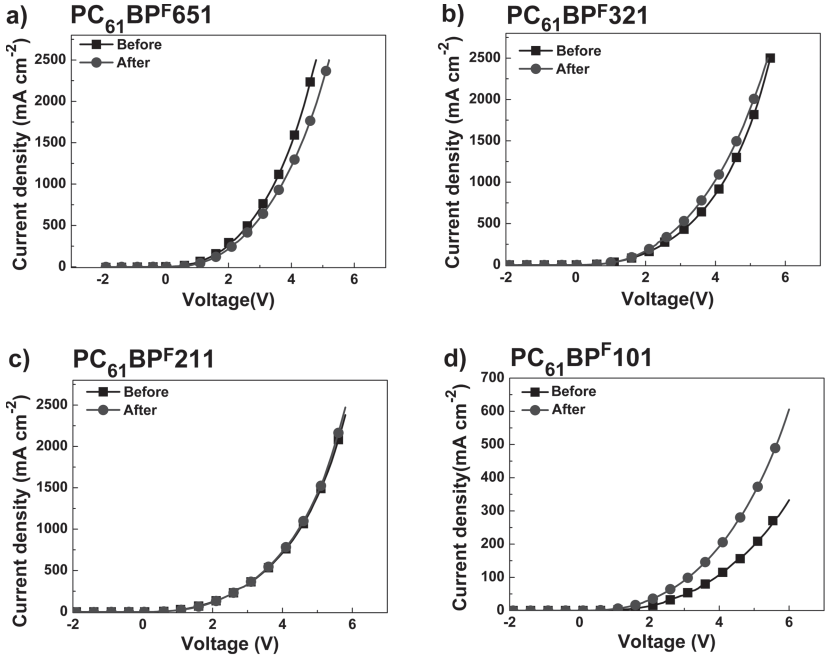

Figure 8. Electron-only devices for a) $PC_{61}BP^F651$, b) $PC_{61}BP^F321$, c) $PC_{61}BP^F211$, and d) $PC_{61}BP^F101$ blends before and after thermal annealing at 150 °C for 25 h.

2.7. Morphological Evolutions

To carefully analyze the influence of $PC_{61}BP^F$ in the active layers, we plotted the initial PCEs and the PCEs after heating for 25 h as a function of the $PC_{61}BP^F$ content in the active layers (**Figure 10**). Based on the analyses, we propose mechanisms for the morphological evolution of P3HT:$PC_{61}BM$ and P3HT:$PC_{61}BM$:$PC_{61}BP^F$ blends, respectively in **Figure 11**. Upon thermal annealing of the as-cast P3HT:$PC_{61}BM$ thin films at 140 °C for 15 min, the $PC_{61}BM$ molecules, originally dispersed and intercalated in the P3HT domains (Figure 11a), can freely diffuse out of these mixed regions to aggregate into pure $PC_{61}BM$ clusters. This evolution of $PC_{61}BM$ simultaneously induces more ordered packing of P3HT, leading to an optimized morphology for efficient exciton dissociation and charge transport (Figure 11b). However, prolonged thermal annealing results in overgrowth of the $PC_{61}BM$ aggregates that reduce the percolating electron transport pathways within the mixed

Table 2. Carrier mobilities of the blends extracted from space-charge limited current method before and after thermal annealing at 150 °C for 25 h.

	$PC_{61}BP^F651$ before	$PC_{61}BP^F651$ after	$PC_{61}BP^F321$ before	$PC_{61}BP^F321$ after	$PC_{61}BP^F211$ before	$PC_{61}BP^F211$ after	$PC_{61}BP^F101$ before	$PC_{61}BP^F101$ after
Electron mobility, μ_e [$cm^2\ s^{-1}\ V^{-1}$]	2.35×10^{-5}	2×10^{-5}	1.78×10^{-5}	2.47×10^{-5}	3.96×10^{-5}	4.11×10^{-5}	1.59×10^{-5}	2.90×10^{-5}
Hole mobility, μ_h, [$cm^2\ s^{-1}\ V^{-1}$]	9.16×10^{-6}	3.44×10^{-5}	5.64×10^{-6}	2.26×10^{-5}	1.27×10^{-5}	3.27×10^{-5}	9.53×10^{-6}	4.94×10^{-5}
Ratio μ_h / μ_e	0.39	1.72	0.23	1.27	0.32	0.80	0.60	1.70

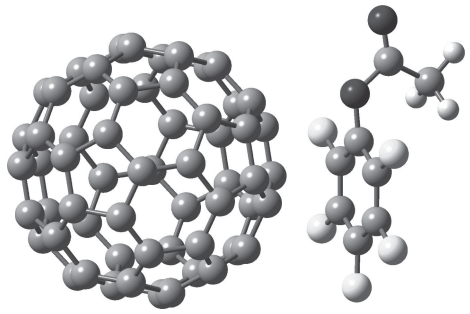

Figure 9. Side view of the optimized structure of $C_{60}BP^F$.

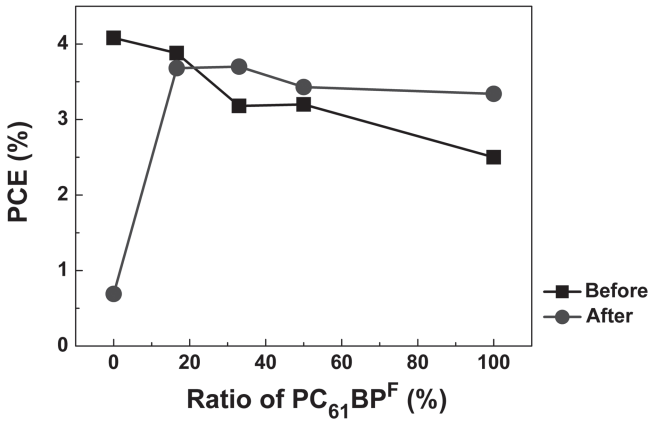

Figure 10. The PCE values as a funtion of the wt% content of $PC_{61}BP^F$ in the active layers. (0 wt% for $PC_{61}BP^F110$, 8.3 wt% for $PC_{61}BP^F651$, 16.6 wt% for $PC_{61}BP^F321$, 25 wt% for $PC_{61}BP^F211$, 50 wt% for $PC_{61}BP^F101$) before and after thermal annealing at 150 °C for 25 h.

regions and thus adversely enhances charge recombination losses (Figure 13c). Although the device $PC_{61}BP^F110$ without $PC_{61}BP^F$ achieved the highest PCE value of 4.08% at the beginning, its morphological stability against heating turns out to be the worst.

For the as-cast $PC_{61}BP^F101$ (50 wt%), $PC_{61}BP^F211$ (25 wt%), and $PC_{61}BP^F321$ (16.6 wt%) thin films (Figure 11a′), aggregation of the fullerene molecules dispersed in the mixed regions is partially restricted by the intermolecular C_6F_5–C_{60} interactions. Pre-annealing at 140 °C for 15 min is therefore not sufficient to achieve optimized morphology (Figure 11b′). By further heating at 150 °C during 25 h, the fullerene molecules in the mixed regions might gradually overcome the supramolecular attractions and slowly aggregate into fullerene clusters with concomitant enhancement of P3HT crystallinity (Figure 11c′). As a result, we observed marginal enhancement of electron mobilities (i.e., $PC_{61}BP^F321$, $PC_{61}BP^F211$ and $PC_{61}BP^F101$) and appreciable improvement of hole mobilities of the blends. In short, the morphologies of the $PC_{61}BP^F$-containing blends are not degraded upon thermal heating but gradually evolved toward the optimal state.

However, when the content of $PC_{61}BP^F$ in the n-type materials is only 8.3 wt% (i.e., $PC_{61}BP^F651$), the suitable morphology can be achieved more easily at an early stage, delivering a PCE of 3.88% (Figure 10). Despite constant heat drove the original morphology away from its optimized state, only a small amount of $PC_{61}BP^F$ can effectively mitigate this negative evolution process. Even after 150 °C heating for 25 h, more than 95% of its initial PCE can be retained.

2.8. PDTBCDTBT:$PC_{71}BM$ Blending System

Recent research on morphological stability of BHJ solar cells is mainly focused on the typical P3HT:$PC_{61}BM$ system. The use of other low band-gap polymers has not been extensively investigated. After successfully demonstrating that $PC_{61}BP^F$ can effectively stabilize the morphology of the P3HT:$PC_{61}BM$-based system, it is envisioned that this strategy could be a general approach applicable to other blending systems using a low band-gap polymer with better molecular properties. A crystalline p-type polymer poly(dithienobenzocarbazole-*alt*-dithienylbenzothiadiazole) (**PDTBCDTBT**) is selected to test this idea (Scheme 1).[24] A device (ITO/PEDOT:PSS/**PDTBCDTBT**:$PC_{71}BM$ (2:3 in wt%)/Ca/Al), where the active layer was thermally annealed at 100 °C for 10 min, achieved a high efficiency of 5.34%. Unfortunately,

Table 3. BP86-BJDAMP/TZP ETS-NOCV analysis of the interaction between C_{60} and BP^F in kcal mol^{-1}. Percentages of total stabilization are given in parentheses.

	ΔE	ΔE_{prep}	ΔE_{int}	ΔE_{pauli}	ΔV_{elst}	ΔE_{oi}	ΔE_{dis}
$C_{60}BP^F$	–9.12	0.32	–9.45	12.91	–5.20 (23%)	–4.05 (18%)	–13.10 (59%)

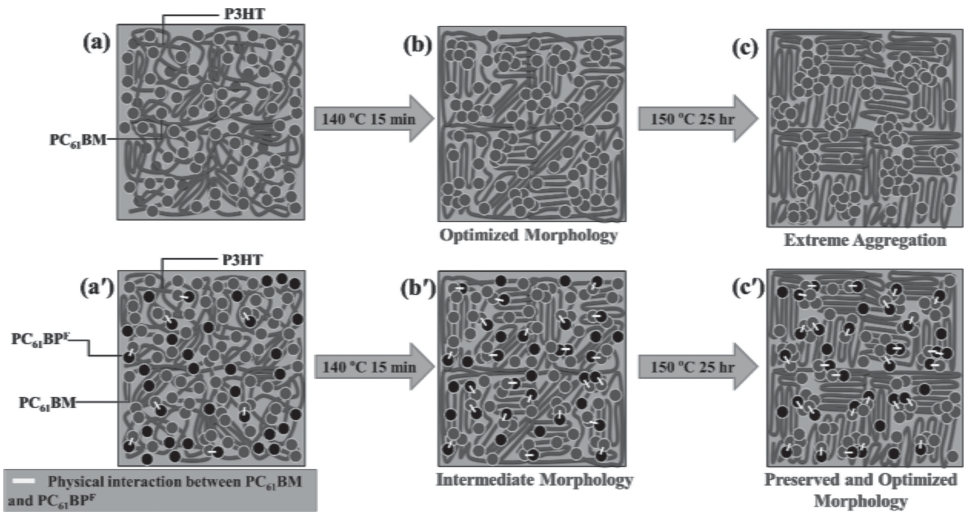

Figure 11. Morphological evolutions of P3HT:$PC_{61}BM$ blend and P3HT:$PC_{61}BM$:$PC_{61}BP^F$ (3:2:1 in wt%) blend. a–c) Unstable morphology of a P3HT:$PC_{61}BM$ binary blend upon thermal heating, and a′–c′) utilization of C_6F_5–C_{60} interactions to stabilize the morphology against thermal heating.

after isothermal heating of the active layer at 150 °C for 24 h, the efficiency dramatically degraded to an extremely low value of 0.01%. A device using ITO/PEDOT:PSS/**PDTBCDTBT**:PC_{71}BM:$PC_{61}BP^F$ (4:5:1 in wt%)/Ca/Al configuration was fabricated by adding 10 wt% $PC_{61}BP^F$ into the active layer. Encouragingly, under otherwise identical conditions, this device delivered an initial efficiency of 5.24% (**Table 4**), indicating that the incorporation of $PC_{61}BP^F$ into this system does not alter the device performance. Most importantly, after thermal annealing at 150 °C for 25 h, the $PC_{61}BP^F$-incorporated device still achieved a comparable PCE of 4.24%, that is about 81% of its original value. This example demonstrates the general capability of $PC_{61}BP^F$ to thermally stabilize the morphology and preserve the efficiency. It should be mentioned that we cannot rule out the possibility of the interaction between the pentafluorophenyl moieties and the electron-rich segments of the polymer. Even though this interaction exists, it is still beneficial for the morphological stability, considering that such interactions should prevent the phase separation between the polymer and fullerene.

This experiment also demonstrates that $PC_{61}BP^F$ is effective not only for $PC_{61}BM$-based system but also for $PC_{71}BM$-based system. To the best of our knowledge, this is the first non-P3HT blend system that shows excellent morphological stability against thermal heating.

Table 4. Photovoltaic parameters of PSCs (ITO/PEDOT:PSS/active layer/Ca/Al) before and after isothermal heating at 150 °C.

Devices	Time [h]	V_{oc} [V]	J_{sc} [mA cm^{-2}]	FF [%]	PCE [%]
PDTBCDTBT:$PC_{71}BM$	0	0.80	–10.28	64.9	5.34
PDTBCDTBT:$PC_{71}BM$	25	1.34	–0.05	20.4	0.01
PDTBCDTBT:$PC_{71}BM$:$PC_{61}BP^F$ (4:5:1 in wt%)	0	0.78	–10.21	65.8	5.24
PDTBCDTBT:$PC_{71}BM$:$PC_{61}BP^F$ (4:5:1 in wt%)	25	0.78	–8.62	63.0	4.24

3. Conclusions

In this study, we have easily synthesized a novel $PC_{61}BM$-based fullerene, [6,6]-phenyl-C_{61} butyric acid pentafluorophenyl ester ($PC_{61}BP^F$). The merit of $PC_{61}BP^F$ molecular design is to impart complementary attraction between the pentafluorophenyl group of $PC_{61}BP^F$ and the C_{60} cores of $PC_{61}BP^F$/$PC_{61}BM$. Such a supramolecular interaction can effectively suppress the n-type $PC_{61}BP^F$/$PC_{61}BM$ materials from extensive thermal-driven aggregation to overcome the morphological instability. Therefore, prolonged thermal annealing at elevated temperatures gradually improves the polymer hole mobility while maintaining sufficient fullerene percolation within the polymer matrix for electron transport. The extent of the physical interaction in bulk can be adjustable by simply varying the content of $PC_{61}BP^F$. By doping only 8.3 wt% $PC_{61}BP^F$, the device $PC_{61}BP^F$651 yielded a PCE of 3.68% after 25 h heating at 150 °C, preserving 95% of its original value. In sharp contrast, the PCE of the device using a traditional P3HT:$PC_{61}BM$ blend decayed drastically to 0.69% over 25 h heating. When $PC_{61}BP$ with non-fluorinated phenyl group was used to substitute the fluorinated $PC_{61}BP^F$, the feature of morphological stabilization disappeared completely. Most significantly, $PC_{61}BP^F$ is also capable of mitigating morphological evolution of another blend system incorporating a conjugated polymer PDTBCDTBT to stabilize the device performance. We envision that this strategy will inspire new design of additive materials that can control BHJ morphology through supramolecular interactions to realize highly efficient and thermally stable solar cells.

4. Experimental Section

General Measurement and Characterization: All chemicals were purchased from Aldrich and Acros, unless otherwise specified. ^1H and ^{13}C spectra were recorded on Varian Unity-300 and 400 spectrometers. Differential scanning calorimetry (DSC) was measured on TA Q200

Instrument under nitrogen atmosphere at a heating rate of 10 °C min^{-1} and thermogravimetric analysis (TGA) was recorded on a Perkin-Elmer Pyris system under nitrogen atmosphere at a heating rate of 20 °C min^{-1}. Absorption spectra were collected on a Hitachi U-4100 spectrophotometer. Electrochemical cyclic voltammetry (CV) was conducted on a CH Instruments electrochemical analyzer at a scanning rate of 100 mV s^{-1}. A carbon glass was used as the working electrode, Pt wire was used as the counter electrode, and Ag/Ag^+ electrode (0.01 M $AgNO_3$, 0.1 M TBAP in acetonitrile) was used as the reference electrode, while 0.1 M tetrabutylammonium hexafluorophosphate in *o*-dichlorobenzene/acetonitrile (4:1) was the electrolyte. The LUMO energy levels were obtained from the equation LUMO = $-(E_{red}^{on} + 4.75)$ eV, where E_{red}^{on} is the onset reduction potential (in volts) versus Ag/Ag^+. The AFM images under tapping mode were taken on Agilent 5500 system. The optical microscopy images were measured by Zeiss Axiophot.

XRD Measurement: Blends of $PC_{61}BP^F110$, $PC_{61}BP^F101$ and $PC_{61}BP^F321$, $PC_{61}BM$, and $PC_{61}BP^F$ were dissolved in 1,2-dichlorobenzene, and drop-cast on glass substrates. The cast films were first characterized with a powder diffractometer (Bruker D8 Advance operated at 40 kV and 40 mA; Cu Kα: λ = 1.5418 Å). The samples were scanned in reflection across a 2θ ranging from 4° to 35° with a step size of 0.07° and a counting period of 1 s $step^{-1}$ to obtain the 1D WAXD patterns of the as-cast films. The tested films were then annealed at 150 °C for 25 h in a glove box and characterized again with the diffractometer to generate the 1D WAXD patterns for the annealed samples.

Device Fabrication and Characterization: Indium tin oxide (ITO)-coated glass substrates were ultrasonically washed by detergent, de-ionic water, acetone and isopropanol sequentially for 15 min/each and then cleaned by UV-ozone for another 15 min. PEDOT:PSS (Baytron PVP AI-4083) was filtered and spin-cast on a cleaned ITO-coated glass at 2000 rpm for 40 s to produce a 30 nm thick PEDOT:PSS interlayer, followed by baking at 170 °C under nitrogen atmosphere. Active-layer solutions with various ratios of P3HT: $PC_{61}BM$: $PC_{61}BP^F$ in *o*-dichlorobenzene were prepared. The weight ratio of P3HT to the n-type materials ($PC_{61}BM$ and $PC_{61}BP^F$ or $PC_{61}BP$) was kept to 1:1 and the concentration of P3HT or fullerene ($PC_{61}BM$ and $PC_{61}BP^F$ or $PC_{61}BP$) remained 1.3 wt%. The individual solutions were stirred at 60 °C for 8 h under nitrogen atmosphere and filtered with a 0.45 μm Teflon syringe filter. They were then spin-coated on top of the PEDOT:PSS layer at 450 rpm for 30 s, respectively. Each resultant film was covered in a Petri dish for 15 min to undergo solvent annealing. For thermal treatment, the film was further baked at 150 °C for different time periods (15 min, 5 h, 10 h, 15 h, 20 h, and 25 h) to give a series of active layers with various thermal annealing time periods. The top electrode (Ca 35 nm/Al 100 nm) was then thermally evaporated at pressure below 10^{-6} Torr to finish the BHJ solar-cell device fabrication. All the devices contained an active area of 0.04 cm^2 and were measured at room temperature under normal atmosphere with a Xenon lamp coupled to an AM1.5G solar filter (SAN-EIXES-301S solar simulator). *J–V* characteristics were recorded with a Keitheley 2400 Source Measurement Unit. For SCLC device fabrication, the top electrode was changed from Ca (35 nm)/Al (100 nm) to Au (40 nm) for hole mobility measurements. For electron mobility measurements, the PEDOT:PSS interlayer was replaced with Al (100 nm). The electron mobilities were calculated according to space-charge-limited-current theory (SCLC). The *J–V* curves were fitted according to the following equation: $J = (9/8)\ \varepsilon\mu\ (V^2/L^3)$ where ε is the permittivity of the blend film, μ the hole mobility, and L the film thickness.

Supporting Information

Synthetic procedures, DSC measurement of $PC_{61}BP^F$, absorption spectra, cyclic voltammetry, TGA measurement of $PC_{61}BP^F$, 1D WAXD of thin films, detailed photovoltaic parameters, computational details, and ^1H and ^{13}C NMR spectra of $PC_{61}BP^F$. Supporting Information is available from the Wiley Online Library or from the author.

Acknowledgement

The authors thank the National Science Council and the "ATU Program" of the Ministry of Education, and Center for Interdisciplinary Science (CIS) of the National Chiao Tung University, Taiwan, for financial support. The authors are grateful to the National Center for High-performance Computing (NCHC) in Taiwan for computer time and facilities. The authors also thank Prof. Yuan-Pern Lee for the support of the AFM measurements.

Received: February 3, 2013
Revised: June 10, 2013
Published online: October 11, 2013

[1] a) Y.-J. Cheng, S.-H. Yang, C.-S. Hsu, *Chem. Rev.* **2009**, *109*, 5868; b) C. J. Brabec, N. S. Sariciftci, J. C. Hummelen, *Adv. Funct. Mater.* **2001**, *11*, 15; c) G. Dennler, M. C. Scharber, C. J. Brabec, *Adv. Mater.* **2009**, *21*, 1323; d) B. C. Thompson, J. M. J. Fréchet, *Angew.Chem., Int. Ed.* **2008**, *47*, 58; e) H.-Y. Chen, J. Hou, S. Zhang, Y. Liang, G. Yang, Y. Yang, L. Yu, Y. Wu, G. Li, *Nat. Photonics* **2009**, *3*, 649; f) G. Yu, J. Gao, J. C. Hummelen, F. Wudl, A. J. Heeger, *Science* **1995**, *270*, 1789; g) G. Li, V. Shrotriya, J. Huang, Y. Yao, T. Moriarty, K. Emery, Y. Yang, *Nat. Mater.* **2005**, *4*, 864; h) J. Chen, Y. Cao, *Acc. Chem. Res.* **2009**, *42*, 1709.

[2] a) G. F. Burkhard, E. T. Hoke, S. R. Scully, M. D. McGehee, *Nano Lett.* **2009**, *9*, 4037; b) W. Ma, C. Yang, X. Gong, K. Lee, A. J. Heeger, *Adv. Funct. Mater.* **2005**, *15*, 1617; c) H. Xin, O. G. Reid, G. Ren, F. S. Kim, D. S. Ginger, S. A. Jenekhe, *ACS Nano* **2010**, *4*, 1861; d) D. R. Kozub, K. Vakhshouri, L. M. Orme, C. Wang, A. Hexemer, E. D. Gomez, *Macromolecules* **2011**, *44*, 5722; e) M. Campoy-Quiles, T. Ferenczi, T. Agostinelli, P. G. Etchegoin, Y. Kim, T. D. Anthopoulos, P. N. Stavrinou, D. D. C. Bradley, J. Nelson, *Nat. Mater.* **2008**, *7*, 158; f) D. C. Coffey, O. G. Reid, D. B. Rodovsky, G. P. Bartholomew, D. S. Ginger, *Nano Lett.* **2007**, *7*, 738.

[3] a) Y. Kim, S. Cook, S. M. Tuladhar, S. A. Choulis, J. Nelson, J. R. Durrant, D. D. C. Bradley, M. Giles, I. McCulloch, C.-S. Ha, M. Ree, *Nat. Mater.* **2006**, *5*, 197; b) M. Reyes-Reyes, K. Kim, J. Dewald, R. López-Sandoval, A. Avadhanula, S. Curran, D. L. Carroll, *Org. Lett.* **2005**, *7*, 5749; c) M. Reyes-Reyes, K. Kim, D. L. Carroll, *Appl. Phys. Lett.* **2005**, *87*, 083506.

[4] a) F. Padinger, R. S. Rittberger, N. S. Sariciftci, *Adv. Funct. Mater.* **2003**, *13*, 85; b) L. H. Nguyen, H. Hoppe, T. Erb, S. Günes, G. Gobsch, N. S. Sariciftci, *Adv. Funct. Mater.* **2007**, *17*, 1071; c) H. Hoppe, T. Glatzel, M. Niggemann, A. Hinsch, M. C. Lux-Steiner, N. S. Sariciftci, *Nano Lett.* **2005**, *5*, 269; d) G. Li, Y. Yao, H. Yang, V. Shrotriya, G. Yang, Y. Yang, *Adv. Funct. Mater.* **2007**, *17*, 1636; e) A. L. Ayzner, D. D. Wanger, C. J. Tassone, S. H. Tolbert, B. J. Schwartz, *J. Phys. Chem. C* **2008**, *112*, 18711; f) N. D. Treat, M. A. Brady, G. Smith, M. F. Toney, E. J. Kramer, C. J. Hawker, M. L. Chabinyc, *Adv. Energy Mater.* **2011**, *1*, 82.

[5] a) E. Klimov, W. Li, X. Yang, G. G. Hoffmann, J. Loos, *Macromolecules* **2006**, *39*, 4493; b) Y.-C. Huang, S.-Y. Chuang, M.-C. Wu, H.-L. Chen, C.-W. Chen, W.-F. Su, *J. Appl. Phys.* **2009**, *106*, 034506/1; c) H. Zhong, X. Yang, B. deWith, J. Loos, *Macromolecules* **2005**, *39*, 218; d) X. Yang, J. K. J. van Duren, R. A. J. Janssen, M. A. J. Michels, J. Loos, *Macromolecules* **2004**, *37*, 2151; e) A. Swinnen, I. Haeldermans, M. van de Ven, J. D'Haen, G. Vanhoyland, S. Aresu, M. D'Olieslaeger, J. Manca, *Adv. Funct. Mater.* **2006**, *16*, 760; f) C. Müller, T. A. M. Ferenczi, M. Campoy-Quiles, J. M. Frost, D. D. C. Bradley, P. Smith, N. Stingelin-Stutzmann, J. Nelson, *Adv. Mater.* **2008**, *20*, 3510.

[6] X. Yang, J. K. J. van Duren, M. T. Rispens, J. C. Hummelen, R. A. J. Janssen, M. A. J. Michels, J. Loos, *Adv. Mater.* **2004**, *16*, 802.

[7] a) M. Jørgensen, K. Norrman, F. C. Krebs, *Sol. Energy Mater. Sol. Cells* **2008**, *92*, 686; b) J. A. Bartelt, Z. M. Beiley, E. T. Hoke, W. R. Mateker, J. D. Douglas, B. A. Collins, J. R. Tumbleston, K. R. Graham, A. Amassian, H. Ade, J. M. J. Fréchet, M. F. Toney, M. D. McGehee, *Adv. Energy Mater.* **2013**, *3,* 364; c) J. M. Kroon, M. M. Wienk, W. J. H. Verhees, J.C. Hummelen, *Thin Solid Films* **2002**, *403*, 223.

[8] a) K. Sivula, C. K. Luscombe, B. C. Thompson, J. M. J. Fréchet, *J. Am. Chem. Soc.* **2006**, *128*, 13988; b) S. Bertho, B. Campo, F. Piersimoni, D. Spoltore, J. D'Haen, L. Lutsen, W. Maes, D. Vanderzande, J. Manca, *Sol. Energy Mater. Sol. Cells* **2013**, *110*, 69.

[9] a) Y. Zhang, H.-L. Yip, O. Acton, S. K. Hau, F. Huang, A. K. Y. Jen, *Chem. Mater.* **2009**, *21*, 2598; b) Y.-J. Cheng, M.-H. Liao, C.-Y. Chang, W.-S. Kao, C.-E. Wu, C.-S. Hsu, *Chem. Mater.* **2011**, *23*, 4056; c) C.-Z. Li, S.-C. Chien, H.-L. Yip, C.-C. Chueh, F.-C. Chen, Y. Matsuo, E. Nakamura, A. K. Y. Jen, *Chem. Commun.* **2011**, *47*, 10082.

[10] a) J. Vandenbergh, B. Conings, S. Bertho, J. Kesters, D. Spoltore, S. Esiner, J. Zhao, G. Van Assche, M. M. Wienk, W. Maes, L. Lutsen, B. Van Mele, R. A. J. Janssen, J. Manca, D. J. M. Vanderzande, *Macromolecules* **2011**, *44*, 8470; b) S. Bertho, G. Janssen, T. J. Cleij, B. Conings, W. Moons, A. Gadisa, J. D'Haen, E. Goovaerts, L. Lutsen, J. Manca, D. Vanderzande, *Sol. Energy Mater. Sol. Cells* **2008**, *92*, 753.

[11] K. Sivula, Z. T. Ball, N. Watanabe, J. M. J. Fréchet, *Adv. Mater.* **2006**, *18*, 206.

[12] a) B. J. Kim, Y. Miyamoto, B. Ma, J. M. J. Fréchet, *Adv. Funct. Mater.* **2009**, *19*, 2273; b) B. Gholamkhass, S. Holdcroft, *Chem. Mater.* **2010**, *22*, 5371; c) Z. Zhu, S. Hadjikyriacou, D. Waller, R. Gaudiana, *J. Macromol. Sci., Part A: Pure Appl. Chem.* **2004**, *41*, 1467; d) M. Drees, H. Hoppe, C. Winder, H. Neugebauer, N. S. Sariciftci, W. Schwinger, F. Schaffler, C. Topf, M. C. Scharber, Z. Zhu, R. Gaudiana, *J. Mater. Chem.* **2005**, *15*, 5158; e) J.-F. Nierengarten, S. Setayesh, *New J. Chem.* **2006**, *30*, 313; f) Y.-J. Cheng, C.-H. Hsieh, P.-J. Li, C.-S. Hsu, *Adv. Funct. Mater.* **2011**, *21*, 1723; g) H. J. Kim, A. R. Han, C.-H. Cho, H. Kang, H.-H. Cho, M. Y. Lee, J. M. J. Fréchet, J. H. Oh, B. J. Kim, *Chem. Mater.* **2011**, *24*, 215.

[13] a) K. R. Graham, P. M. Wieruszewski, R. Stalder, M. J. Hartel, J. Mei, F. So, J. R. Reynolds, *Adv. Funct. Mater.* **2012**, *22*, 4801; b) J. K. Lee, W. L. Ma, C. J. Brabec, J. Yuen, J. S. Moon, J. Y. Kim, K. Lee, G. C. Bazan, A. J. Heeger, *J. Am. Chem. Soc.* **2008**, *130*, 3619; c) S. J. Lou, J. M. Szarko, T. Xu, L. Yu, T. J. Marks, L. X. Chen, *J. Am. Chem. Soc.* **2011**, *133*, 20661; d) C. V. Hoven, X.-D. Dang, R. C. Coffin, J. Peet, T.-Q. Nguyen, G. C. Bazan, *Adv. Mater.* **2010**, *22*, E63; e) T. Salim, L. H. Wong, B. Brauer, R. Kukreja, Y. L. Foo, Z. Bao, Y. M. Lam, *J. Mater. Chem.* **2011**, *21*, 242; f) J. T. Rogers, K. Schmidt, M. F. Toney, G. C. Bazan, E. J. Kramer, *J. Am. Chem. Soc.* **2012**, *134*, 2884; g) A. T. Yiu, P. M. Beaujuge, O. P. Lee, C. H. Woo, M. F. Toney, J. M. J. Fréchet, *J. Am. Chem. Soc.* **2011**, *134*, 2180; h) H. Xin, X. Guo, G. Ren, M. D. Watson, S. A. Jenekhe, *Adv. Energy Mater.* **2012**, *2*, 575; i) C.-Y. Chang, Y.-J. Cheng, S.-H. Hung, J.-S. Wu, W.-S. Kao, C.-H. Lee, C.-S. Hsu, *Adv. Mater.* **2012**, *24*, 549; j) J. Peet, J. Y. Kim, N. E. Coates, W. L. Ma, D. Moses, A. J. Heeger, G. C. Bazan, *Nat. Mater.* **2007**, *6*, 497.

[14] a) M. T. Rispens, L. Sanchez, J. Knol, J. C. Hummelen, *Chem. Commun.* **2001**, 161; b) L. Sanchez, M. T. Rispens, J. C. Hummelen, *Angew. Chem., Int. Ed.* **2002**, *41*, 838; c) C.-C. Chu, G. Raffy, D. Ray, A. D. Guerzo, B. Kauffmann, G. Wantz, L. Hirsch, D. M. Bassani, *J. Am. Chem. Soc.* **2010**, *132*, 12717; d) M. Murakami, K. Ohkubo, T. Hasobe, V. Sgobba, D. M. Guldi, F. Wessendorf, A. Hirsch, S. Fukuzumi, *J. Mater. Chem.* **2010**, *20*, 1457; e) L. Sanchez, N. Martin, D. M. Guldi, *Angew. Chem., Int. Ed.* **2005**, *44*, 5374; f) U. Hahn, J. J. Gonzalez, E. Huerta, M. Segura, J.-F. Eckert, F. Cardinali, M. J. de, J.-F. Nierengarten, *Chem. Eur. J.* **2005**, *11*, 6666.

[15] S.-L. Hsu, C.-M. Chen, Y.-H. Cheng, K.-H. Wei, *J. Polym. Sci., Part A: Polym. Chem.* **2011**, *49*, 603.

[16] a) C. R. Patrick, G. S. Prosser, *Nature* **1960**, *187*, 1021; b) X.-H. Zhou, J. Luo, S. Huang, T.-D. Kim, Z. Shi, Y.-J. Cheng, S.-H. Jang, D. B. Knorr, R. M. Overney, A. K. Y. Jen, *Adv. Mater.* **2009**, *21*, 1976; c) G. W. Coates, A. R. Dunn, L. M. Henling, J. W. Ziller, E. B. Lobkovsky, R. H. Grubbs, *J. Am. Chem. Soc.* **1998**, *120*, 3641; d) T. Gray, T.-D. Kim, D. B. Knorr, Jr., J. Luo, A. K. Y. Jen, R. M. Overney, *Nano Lett.* **2008**, *8*, 754; e) E. A. Meyer, R. K. Castellano, F. Diederich, *Angew. Chem., Int. Ed.* **2003**, *42*, 1210; f) M. L. Renak, G. P. Bartholomew, S. Wang, P. J. Ricatto, R. J. Lachicotte, G. C. Bazan, *J. Am. Chem. Soc.* **1999**, *121*, 7787; g) L. M. Salonen, M. Ellermann, F. Diederich, *Angew. Chem., Int. Ed.* **2011**, *50*, 4808; h) A. F. M. Kilbinger, R. H. Grubbs, *Angew. Chem., Int. Ed.* **2002**, *41*, 1563.

[17] C.-Z. Li, Y. Matsuo, T. Niinomi, Y. Sato, E. Nakamura, *Chem. Commun.* **2010**, *46*, 8582.

[18] a) T. J. Prosa, M. J. Winokur, J. Moulton, P. Smith, A. J. Heeger, *Macromolecules* **1992**, *25*, 4364; b) N. Kayunkid, S. Uttiya, M. Brinkmann, *Macromolecules* **2010**, *43*, 4961.

[19] J. Zhao, A. Swinnen, G. Van Assche, J. Manca, D. Vanderzande, B. V. Mele, *J. Phys. Chem. B* **2009**, *113*, 1587.

[20] D. E. Motaung, G. F. Malgas, C. J. Arendse, S. E. Mavundla, C. J. Oliphant, D. Knoesen, *J. Mater. Sci.* **2009**, *44*, 3192.

[21] J.-D. Chai, M. Head-Gordon, *Phys. Chem. Chem. Phys.* **2008**, *10*, 6615.

[22] a) M. Mitoraj, A. Michalak, *J. Mol. Model.* **2007**, *13*, 347; b) M. Mitoraj, A. Michalak, *Organometallics* **2007**, *26*, 6576; c) M. Mitoraj, A. Michalak, *J. Mol. Model.* **2008**, *14*, 681; d) A. Michalak, M. Mitoraj, T. Ziegler, *J. Phys. Chem. A* **2008**, *112*, 1933; e) M. P. Mitoraj, A. Michalak, T. Ziegler, *J. Chem. Theory Comput.* **2009**, *5*, 962; f) M. P. Mitoraj, A. Michalak, T. Ziegler, *Organometallics* **2009**, *28*, 3727; g) M. Srebro, M. Mitoraj, A. Michalak, *Can. J. Chem.* **2009**, *87*, 1039; h) M. Mitoraj, M. Parafiniuk, M. Srebro, M. Handzlik, A. Buczek, A. Michalak, *J. Mol. Model.* **2011**, *17*, 2337; i) E. Broclawik, J. Załucka, P. Kozyra, M. Mitoraj, J. Datka, *Catal. Today* **2011**, *169*, 45; j) M. P. Mitoraj, A. Michalak, *Inorg. Chem.* **2011**, *50*, 2168; k) M. Mitoraj, R. Kurczab, M. Boczar, A. Michalak, *J. Mol. Model.* **2010**, *16*, 1789; l) M. Srebro, M. Mitoraj, *Organometallics* **2009**, *28*, 3650; m) M. P. Mitoraj, H. Zhu, A. Michalak, T. Ziegler, *Int. J. Quantum Chem.* **2009**, *109*, 3379; n) R. Kurczab, M. P. Mitoraj, A. Michalak, T. Ziegler, *J. Phys. Chem. A* **2010**, *114*, 8581.

[23] a) S. Grimme, J. Antony, S. Ehrlich, H. Krieg, *J. Chem. Phys.* **2010**, *132*, 154104; b) S. Grimme, S. Ehrlich, L. Goerigk, *J. Comput. Chem.* **2011**, *32*, 1456–1465.

[24] J.-S. Wu, Y.-Y. Lai, Y.-J. Cheng, C.-Y. Chang, C.-L. Wang, C.-S. Hsu, *Adv. Energy Mater.* **2013**, *3*, 457.